Journal of Marine Science and Technology

Volume 18 | Issue 1 Article 2

SHAPE OPTIMIZATION OF ONE-CHAMBER MUFFLERS WITH REVERSE-FLOW DUCTS USING A GENETIC ALGORITHM

Min-Chie Chiu
Department of Automatic Control Engineering, Chungchou Institute of Technology, Changhua County, Taiwan, R.O.C., minchie.chiu@msa.hinet.net

SHAPE OPTIMIZATION OF ONE-CHAMBER MUFFLERS WITH REVERSE-FLOW DUCTS USING A GENETIC ALGORITHM

Acknowledgements

The author acknowledges the financial support of the National Science Council (NSC 95-2218-E-235-002, ROC)

Journal of Marine Science and Technology, Vol. 18, No. 1, pp. 12-23 (2010)

SHAPE OPTIMIZATION OF ONE-CHAMBER MUFFLERS WITH REVERSE-FLOW DUCTS USING A GENETIC ALGORITHM

Min-Chie Chiu*

Key words: reverse-flow, decoupled numerical method, space constraints, genetic algorithm.

ABSTRACT

Shape optimization on mufflers within a limited space is essential for industry where the equipment layout is occasionally tight and the available space for a muffler is limited for maintenance and operation purposes. To proficiently enhance the acoustical performance within a constrained space, the selection of an appropriate acoustical mechanism and optimizer becomes crucial. A one-chamber muffler hybridized with reverse-flow ducts which can visibly increase the acoustical performance is rarely addressed; therefore, the main purpose of this paper is to numerically analyze and maximize the acoustical performance of this muffler within a limited space.

In this paper, the four-pole system matrix for evaluating the acoustic performance — sound transmission loss (*STL*) — is derived by using a decoupled numerical method. Moreover, a genetic algorithm (*GA*), a robust scheme used to search for the global optimum by imitating the genetic evolutionary process, has been used during the optimization process. Before dealing with a broadband noise, the *STL*'s maximization with respect to a one-tone noise is introduced for a reliability check on the *GA* method. Moreover, the accuracy check of the mathematical model is performed.

The optimal result in eliminating broadband noise reveals that the one-chamber muffler with reverse-flow perforated ducts is excellent for noise reduction. Consequently, the approach used for the optimal design of the noise elimination proposed in this study is easy and effective.

I. INTRODUCTION

To overcome the low frequency noise emitted from a venting system, a muffler has been continually used [6]. Research on mufflers was started by Davis *et al.* in 1954 [3]. To increase a muffler's acoustical performance, the assessment of a new acoustical element — a reverse-flow mechanism with double internal perforated tubes — was proposed and investigated by Munjal *et al.* in 1987 [8]. On the basis of coupled differential equations, a series of theories and numerical techniques in decoupling the acoustical problems have been proposed [8, 11, 12, 13, 14]. Considering the flowing effect, Munjal [7] and Peat [9] publicized the generalized decoupling and numerical decoupling methods, which overcome the drawbacks seen in the previous studies.

Because of the necessity of operation and maintenance within an enclosed machine room, a space-constrained problem within a noise abatement facility will occur; therefore, there is a growing need to optimize the acoustical performance within a fixed space. Yet, the need to investigate the optimal muffler design under space constraints is rarely tackled. In previous papers, the shape optimizations of simple-expansion mufflers were discussed [1, 2, 15, 16]. To greatly enlarge the acoustical performance within a fixed space, a new acoustical mechanism of one-chamber mufflers hybridized with reverse-flow perforated tubes using the novel scheme of a genetic algorithm (*GA*) is presented.

In this paper, the *GA* method patterned after the Darwinian notion of natural selection is applied in this work.

II. THEORETICAL BACKGROUND

In this paper, a one-chamber muffler with reverse-flow perforated mufflers was adopted for noise elimination in the air compressor room shown in Fig. 1. The outlines of these mufflers are shown in Fig. 2. Before the acoustical fields of mufflers are analyzed, the acoustical elements have to be distinguished. As shown in Fig. 3, two kinds of muffler components, including two straight ducts and a reverse-flow perforated duct, are identified and symbolized as I and II. In addition, the acoustic pressure $\overline{p}$ and acoustic particle velocity $\overline{u}$ within the muffler are depicted in Fig. 4 where the acoustical field is represented by four nodes.

The muffler system is composed of two kinds of acoustical elements. The individual transfer matrix derivations with respect to two kinds of acoustical mechanisms are described as below.

Paper submitted 06/03/08; revised 08/11/08; accepted 12/13/08. Author for correspondence: Min-Chie Chiu (e-mail: minchie.chiu@msa.hinet.net).
**Department of Automatic Control Engineering, Chungchou Institute of Technology, Changhua County, Taiwan, R.O.C.*

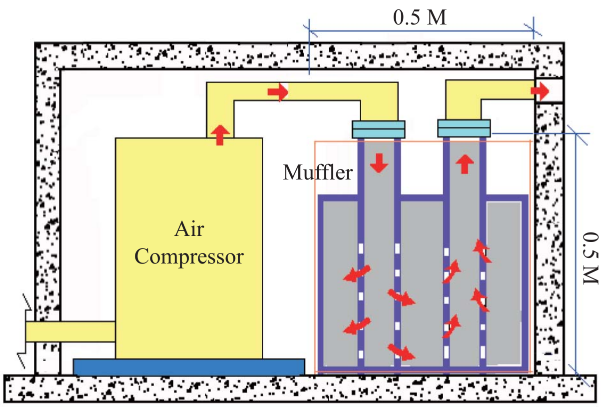

Fig. 1. Noise elimination of an air compressor noise inside a limited space.

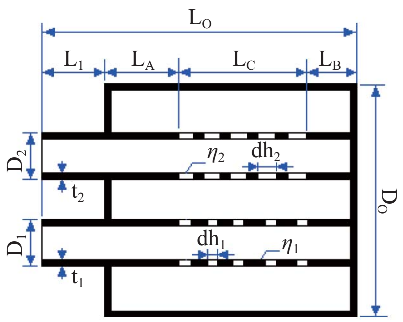

Fig. 2. The outline of a one-chamber muffler with reverse-flow ducts.

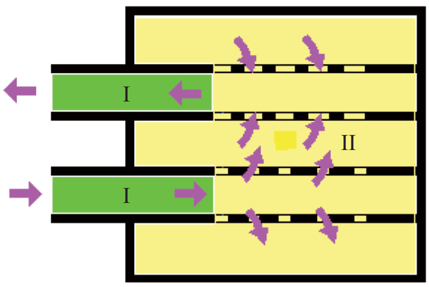

Fig. 3. A distinction in a one-chamber muffler with reverse-flow ducts.

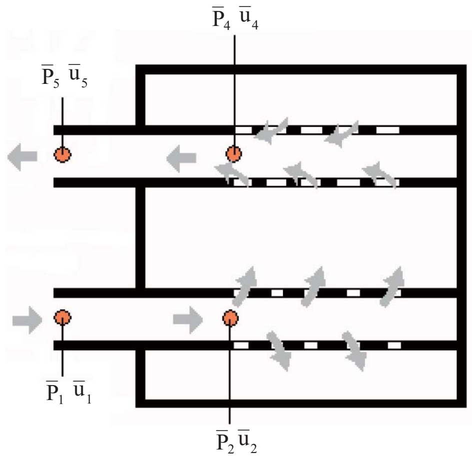

Fig. 4. An acoustical field in a one-chamber muffler with reverse-flow perforated ducts.

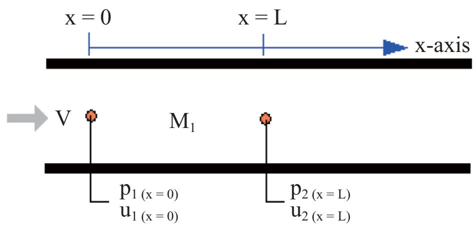

Fig. 5. Sound propagation inside a straight duct.

1. Transfer Matrix of a Straight Duct

For a one dimensional wave propagating in a symmetric straight duct shown in Fig. 5, the acoustic pressure and particle velocity are

$$p(x,t) = \left(c_1 e^{-jkx/(1+M)} + c_2 e^{+jkx/(1-M)}\right) e^{jwt} \tag{1}$$

$$u(x,t) = \left(\frac{c_1}{\rho_o c_o} e^{-jkx/(1+M)} - \frac{c_2}{\rho_o c_o} e^{+jkx/(1-M)}\right) e^{jwt} \tag{2}$$

Considering boundary conditions of pt 1 (x = 0) and pt 2 (x = L), Eqs. (1) and (2) can be rearranged as

$$\begin{pmatrix} p_1(0,0) \\ \rho_o c_o u_1(0,0) \end{pmatrix} = \begin{bmatrix} 1 & 1 \\ 1 & -1 \end{bmatrix} \begin{pmatrix} c_1 \\ c_2 \end{pmatrix} \tag{3}$$

$$\begin{pmatrix} p_1(L,0) \\ \rho_o c_o u_1(L,0) \end{pmatrix} = \begin{bmatrix} e^{-jk^+L} & e^{+jk^-L} \\ e^{-jk^+L} & -e^{+jk^-L} \end{bmatrix} \begin{pmatrix} c_1 \\ c_2 \end{pmatrix} \tag{4a}$$

$$\text{where } k^+ = \frac{k}{1+M_1};\ k^- = \frac{k}{1-M_1} \tag{4b}$$

Combination of (3) and (4) yields

$$\begin{pmatrix} p_1(0,0) \\ \rho_o c_o u_1(0,0) \end{pmatrix} = e^{-j\frac{M_1 kL_1}{1-M_1^2}} \begin{bmatrix} \cos\left(\dfrac{kL_1}{1-M_1^2}\right) & j\sin\left(\dfrac{kL_1}{1-M_1^2}\right) \\ j\sin\left(\dfrac{kL_1}{1-M_1^2}\right) & \cos\left(\dfrac{kL_1)}{1-M_1^2}\right) \end{bmatrix} \begin{pmatrix} p_1(L,0) \\ \rho_o c_o u_1(L,0) \end{pmatrix} \tag{5a}$$

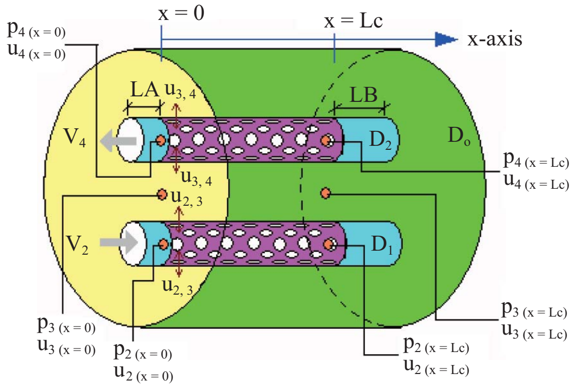

Fig. 6. The mechanism of an acoustical element for a one-chamber muffler with reverse-flow perforated ducts.

or

$$\begin{pmatrix} \bar{p}_1 \\ \rho_o c_o \bar{u}_1 \end{pmatrix} = e^{-j\frac{M_1 kL_1}{1-M_1^2}} \begin{bmatrix} TS_{1,1} & TS_{1,2} \\ TS_{2,1} & TS_{2,2} \end{bmatrix} \begin{pmatrix} \bar{p}_2 \\ \rho_o c_o \bar{u}_2 \end{pmatrix} \tag{5b}$$

where

$$\bar{p}_1 = p_1(0,0);\ \bar{p}_2 = p_1(L,0);\ \bar{u}_1 = u_1(0,0);\ \bar{u}_2 = u_1(L,0);$$

$$TS1_{1,1} = \cos\left[\frac{kL_1}{1-M_1^2}\right];\ TS1_{1,2} = j\sin\left[\frac{kL_1}{1-M_1^2}\right];$$

$$TS1_{2,1} = j\sin\left[\frac{kL_1}{1-M_1^2}\right];\ TS1_{2,2} = \cos\left[\frac{kL_1}{1-M_1^2}\right] \tag{5c}$$

2. Transfer Matrix of a Reverse-flow Perforated Duct

As shown in Fig. 6, there are six nodes located inside the acoustical field. Based on the derivation from Munjal *et al.* [7], the continuity equations and momentum equations with respect to the inner and outer tubes in the first chamber are listed below.

Inner tube 1:
continuity equation

$$V_2 \frac{\partial \rho_2}{\partial x} + \rho_o \frac{\partial u_2}{\partial x} + \frac{4\rho_o}{D_1} u_{2,3} + \frac{\partial \rho_2}{\partial t} = 0 \tag{6}$$

momentum equation

$$\rho_o \left(\frac{\partial}{\partial t} + V_2 \frac{\partial}{\partial x} \right) u_2 + \frac{\partial p_2}{\partial x} = 0 \tag{7}$$

Inner tube 2:
continuity equation

$$V_4 \frac{\partial \rho_4}{\partial x} + \rho_o \frac{\partial u_4}{\partial x} - \frac{4\rho_o}{D_8} u_{3,4} + \frac{\partial \rho_4}{\partial t} = 0 \tag{8}$$

momentum equation

$$\rho_o \left(\frac{\partial}{\partial t} + V_4 \frac{\partial}{\partial x} \right) u_4 + \frac{\partial p_4}{\partial x} = 0 \tag{9}$$

Outer tube:
continuity equation

$$\rho_o \frac{\partial u_3}{\partial x} - V_3 \frac{\partial \rho_3}{\partial x} - \frac{4D_1\rho_o}{D_o^2 - D_1^2 - D_2^2} u_{2,3} + \frac{4D_2}{D_o^2 - D_1^2 - D_2^2} \rho_o u_{2,3}$$

$$+ \frac{\partial \rho_3}{\partial t} = 0 \tag{10}$$

momentum equation

$$\rho_o \left(\frac{\partial}{\partial t} + V_3 \frac{\partial}{\partial x} \right) u_3 + \frac{\partial \rho_3}{\partial x} = 0 \tag{11}$$

Assuming that the acoustic wave is a harmonic motion

$$p(x, t) = P(x) \cdot e^{j\omega t} \tag{12}$$

under the isentropic processes in ducts, it yields

$$P(x) = \rho(x) \cdot c_o^2 \tag{13}$$

Assuming that the perforation along the inner tubes is uniform (ie. $d\xi/dx = 0$), the acoustic impedance of the perforation ($\rho_o\ c_o\ \xi$) is

$$\rho_o\ c_o\ \xi_1 = \frac{p_2(x) - p_3(x)}{u_{2,3}(x)} \tag{14}$$

$$\rho_o\ c_o\ \xi_2 = \frac{p_2(x) - p_3(x)}{u_{2,3}(x)} \tag{15}$$

where ξ_1, ξ_2, are the specific acoustical impedances of the inner perforated tube1 and tube 2, respectively. According to the formula of ξ developed by Sullivan [13] and Rao [10], the empirical formulations for the perforation with or without mean flow are adopted in this study.

For perforates with stationary medium, we have

$$\xi_1 = [0.006 + jk(t_1 + 0.75dh_1)]/\eta_1 \tag{16a}$$

$$\xi_2 = [0.006 + jk(t_2 + 0.75dh_2)]/\eta_2 \tag{16b}$$

For perforates with grazing flow, we have

$$\xi_1 = [0.514 D_1 M_2/(L_C \eta_1) + j0.95k(t_1 + 0.75dh_1)]/\eta_1 \quad (17a)$$

$$\xi_2 = [0.514 D_3 M_4/(L_C \eta_2) + j0.95k(t_2 + 0.75dh_2)]/\eta_2 \quad (17b)$$

where dh_1 and dh_2 are the diameters of the perforated holes on inner tube 1 and tube 2; t_1 and t_2 are the thickness of the inner perforated tube 1 and tube 2; η_1 and η_2 are the porosities of the perforated tube 1 and tube 2.

The available ranges of the above parameters are [10]

$$\text{M: } 0.05 \le M_2, M_4 \le 0.2 \quad (18a)$$

$$\eta\text{: } 0.03 \le \eta_1, \eta_2 \le 0.1 \quad (18b)$$

$$\text{t: } 0.001 \le t_1, t_2 \le 0.003 \quad (18c)$$

$$\text{dh: } 0.00175 \le dh_1, dh_2 \le 0.007 \quad (18d)$$

Eliminating u_2, u_4, $u_{2,3}$, $u_{3,4}$, ρ_2, ρ_3 and ρ_4 using from (6)~(18) yields

$$\begin{bmatrix} D^2+\alpha_1 D+\alpha_2 & \alpha_3 D+\alpha_4 & 0 \\ \alpha_5 D+\alpha_6 & D^2+\alpha_7 D+\alpha_8 & \alpha_9 D+\alpha_{10} \\ 0 & \alpha_{11} D+\alpha_{12} & D^2+\alpha_{13} D+\alpha_{14} \end{bmatrix} \begin{bmatrix} p_2(x) \\ p_3(x) \\ p_4(x) \end{bmatrix} = \begin{bmatrix} 0 \\ 0 \\ 0 \end{bmatrix} \quad (19a)$$

where $D = \dfrac{d}{dx}$ (19b)

$$\alpha_1 = -\frac{jM_2}{1-M_2^2}\left(2k - j\frac{4}{D_1\xi_1}\right) \quad (19c)$$

$$\alpha_2 = \frac{1}{1-M_2^2}\left(k^2 - j\frac{4k}{D_1\xi_1}\right) \quad (19d)$$

$$\alpha_3 = \frac{M_2}{1-M_2^2}\cdot\frac{4}{D_1\xi_1} \quad (19e)$$

$$\alpha_4 = -\frac{j}{1-M_2^2}\cdot\frac{4k}{D_1\xi_1} \quad (19f)$$

$$\alpha_5 = \frac{M_3}{1-M_3^2}\cdot\frac{4D_1}{(D_o^2-D_1^2-D_2^2)\xi_1} \quad (19g)$$

$$\alpha_6 = \frac{j}{1-M_3^2}\cdot\frac{4kD_1}{(D_o^2-D_1^2-D_2^2)\xi_1} \quad (19h)$$

$$\alpha_7 = -\frac{jM_3}{1-M_3^2}\left(2k - \frac{j4D_1}{(D_o^2-D_1^2-D_2^2)\xi_1} - \frac{j4D_2}{(D_o^2-D_1^2-D_2^2)\xi_2}\right) \quad (19i)$$

$$\alpha_8 = \frac{1}{1-M_3}\left(k^2 - \frac{j4kD_1}{(D_o^2-D_1^2-D_2^2)\xi_1} - \frac{j4kD_2}{(D_o^2-D_1^2-D_2^2)\xi_2}\right) \quad (19j)$$

$$\alpha_9 = \frac{M_3}{1-M_3^2}\left(\frac{4D_2}{(D_o^2-D_1^2-D_2^2)\xi_2}\right) \quad (19k)$$

$$\alpha_{10} = \frac{j}{1-M_3^2}\left(\frac{4kD_2}{(D_o^2-D_1^2-D_2^2)\xi_2}\right) \quad (19l)$$

$$\alpha_{11} = \frac{M_4}{1-M_4^2}\left(\frac{4}{D_2\xi_2}\right) \quad (19m)$$

$$\alpha_{12} = \frac{j}{1-M_4^2}\left(\frac{4k}{D_2\xi_2}\right) \quad (19n)$$

$$\alpha_{13} = \frac{-jM_4}{1-M_4^2}\left(2k - j\frac{4}{D_2\xi_2}\right) \quad (19o)$$

$$\alpha_{14} = \frac{1}{1-M_4^2}\left(k^2 - j\frac{4k}{D_2\xi_2}\right) \quad (19p)$$

Developing (19a) yields

$$p_2'' + \alpha_1 p_2' + \alpha_2 p_2 + \alpha_3 p_3' + \alpha_4 p_3 = 0 \quad (20a)$$

$$\alpha_5 p_2' + \alpha_6 p_2 + p_3'' + \alpha_7 p_3' + \alpha_8 p_3 + \alpha_9 p_4' + \alpha_{10} p_4 = 0 \quad (20b)$$

$$\alpha_{11} p_3' + \alpha_{12} p_3 + p_4'' + \alpha_{13} p_4' + \alpha_{14} p_4 = 0 \quad (20c)$$

Let $p_2' = \dfrac{dp_2}{dx} = y_1$, $p_3' = \dfrac{dp_3}{dx} = y_2$, $p_4' = \dfrac{dp_4}{dx} = y_3$,

$$p_2 = y_4,\ p_3 = y_5,\ p_4 = y_6 \quad (21)$$

According to (20) and (21), the new matrix between {y'} and {y} is

$$\begin{bmatrix} y_1' \\ y_2' \\ y_3' \\ y_4' \\ y_5' \\ y_6' \end{bmatrix} = \begin{bmatrix} -\alpha_1 & -\alpha_3 & 0 & -\alpha_2 & -\alpha_4 & 0 \\ -\alpha_5 & -\alpha_7 & -\alpha_9 & -\alpha_6 & -\alpha_8 & -\alpha_{10} \\ 0 & -\alpha_{11} & -\alpha_{13} & 0 & -\alpha_{12} & -\alpha_{14} \\ 1 & 0 & 0 & 0 & 0 & 0 \\ 0 & 1 & 0 & 0 & 0 & 0 \\ 0 & 0 & 1 & 0 & 0 & 0 \end{bmatrix} \begin{bmatrix} y_1 \\ y_2 \\ y_3 \\ y_4 \\ y_5 \\ y_6 \end{bmatrix} \tag{22a}$$

which can be briefly expressed as

$$\{y'\} = [\Lambda]\{y\} \tag{22b}$$

$$\text{Let } \{y\} = [\Pi]\{\Gamma\} \tag{23a}$$

which is

$$\begin{bmatrix} dp_2/dx \\ dp_3/dx \\ dp_4/dx \\ p_2 \\ p_3 \\ p_4 \end{bmatrix} = \begin{bmatrix} \Pi_{1,1} & \Pi_{1,2} & \Pi_{1,3} & \Pi_{1,4} & \Pi_{1,5} & \Pi_{1.6} \\ \Pi_{2,1} & \Pi_{2,2} & \Pi_{2,3} & \Pi_{2,4} & \Pi_{2,5} & \Pi_{2,6} \\ \Pi_{3,1} & \Pi_{3,2} & \Pi_{3,3} & \Pi_{3,4} & \Pi_{3,5} & \Pi_{3,6} \\ \Pi_{4,1} & \Pi_{4,2} & \Pi_{4,3} & \Pi_{4,4} & \Pi_{4,5} & \Pi_{4,6} \\ \Pi_{5,1} & \Pi_{5,2} & \Pi_{5,3} & \Pi_{5,4} & \Pi_{5,5} & \Pi_{5,6} \\ \Pi_{6,1} & \Pi_{6,2} & \Pi_{6,3} & \Pi_{6,4} & \Pi_{6,5} & \Pi_{6,6} \end{bmatrix} \begin{bmatrix} \Gamma_1 \\ \Gamma_2 \\ \Gamma_3 \\ \Gamma_4 \\ \Gamma_5 \\ \Gamma_6 \end{bmatrix} \tag{23b}$$

$[\Pi]_{6x6}$ is the model matrix formed by six sets of eigen vectors Π_{6x1} of $[\Lambda]_{6x6}$.

Combining (23) with (22) and then multiplying $[\Pi]^{-1}$ by both sides, we have

$$[\Pi]^{-1}[\Pi]\{\Gamma'\} = [\Pi]^{-1}[\Lambda][\Pi]\{\Gamma\} \tag{24}$$

Set

$$[\Omega] = [\Pi]^{-1}[\Lambda][\Pi] = \begin{bmatrix} \lambda_1 & 0 & 0 & 0 & 0 & 0 \\ 0 & \lambda_2 & 0 & 0 & 0 & 0 \\ 0 & 0 & \lambda_3 & 0 & 0 & 0 \\ 0 & 0 & 0 & \lambda_4 & 0 & 0 \\ 0 & 0 & 0 & 0 & \lambda_5 & 0 \\ 0 & 0 & 0 & 0 & 0 & \lambda_6 \end{bmatrix} \tag{25}$$

where λ_i is the eigen value of $[\Lambda]$.

Equation (23) can be thus rewritten as

$$\{\Gamma'\} = [\Omega]\{\Gamma\} \tag{26}$$

Obviously, Eq. (26) is a decoupled equation. The related solution yields

$$\Gamma_i = k_i e^{\lambda_i x} \tag{27}$$

Using (7), (9), (11), (23) and (27), the relationship of the acoustic pressure and the particle velocity yields

$$\begin{bmatrix} p_2(x) \\ p_3(x) \\ p_4(x) \\ \rho_o c_o u_2(x) \\ \rho_o c_o u_3(x) \\ \rho_o c_o u_4(x) \end{bmatrix} = \begin{bmatrix} \mathrm{E}_{1,1} & \mathrm{E}_{1,2} & \mathrm{E}_{1,3} & \mathrm{E}_{1,4} & \mathrm{E}_{1,5} & \mathrm{E}_{1,6} \\ \mathrm{E}_{2,1} & \mathrm{E}_{2,2} & \mathrm{E}_{2,3} & \mathrm{E}_{2,4} & \mathrm{E}_{2,5} & \mathrm{E}_{2,6} \\ \mathrm{E}_{3,1} & \mathrm{E}_{3,2} & \mathrm{E}_{3,3} & \mathrm{E}_{3,4} & \mathrm{E}_{3,5} & \mathrm{E}_{3,6} \\ \mathrm{E}_{4,1} & \mathrm{E}_{4,2} & \mathrm{E}_{4,3} & \mathrm{E}_{4,4} & \mathrm{E}_{4,5} & \mathrm{E}_{4,6} \\ \mathrm{E}_{5,1} & \mathrm{E}_{5,2} & \mathrm{E}_{5,3} & \mathrm{E}_{5,4} & \mathrm{E}_{5,5} & \mathrm{E}_{5,6} \\ \mathrm{E}_{6,1} & \mathrm{E}_{6,2} & \mathrm{E}_{6,3} & \mathrm{E}_{6,4} & \mathrm{E}_{6,5} & \mathrm{E}_{6,6} \end{bmatrix} \begin{bmatrix} k_1 \\ k_2 \\ k_3 \\ k_4 \\ k_5 \\ k_6 \end{bmatrix} \tag{28a}$$

$$\text{where } \mathrm{E}_{1,i} = \Pi_{4,i} e^{\lambda_i x} \tag{28b}$$

$$\mathrm{E}_{2,i} = \Pi_{5,i} e^{\lambda_i x} \tag{28c}$$

$$\mathrm{E}_{3,i} = \Pi_{6,i} e^{\lambda_i x} \tag{28d}$$

$$\mathrm{E}_{4,i} = -\frac{e^{\lambda_i x}}{jk + M_2 \lambda_i} \tag{28e}$$

$$\mathrm{E}_{5,i} = -\frac{\Pi_{2,i} e^{\lambda_i x}}{jk + M_3 \lambda_i} \tag{28f}$$

$$\mathrm{E}_{6,i} = -\frac{\Pi_{3,i} e^{\lambda_i x}}{jk + M_4 \lambda_i} \tag{28g}$$

Taking two cases of x = 0 and x = Lc into (28) yields

$$\begin{bmatrix} p_2(0) \\ p_3(0) \\ p_4(0) \\ \rho_o c_o u_2(0) \\ \rho_o c_o u_3(0) \\ \rho_o c_o u_4(0) \end{bmatrix} = [\mathrm{E}(0)] \begin{bmatrix} kf_1 \\ kf_2 \\ kf_3 \\ kf_4 \\ kf_5 \\ kf_6 \end{bmatrix} \tag{29a}$$

$$\begin{bmatrix} p_2(L_C) \\ p_3(L_C) \\ p_4(L_C) \\ \rho_o c_o u_2(L_C) \\ \rho_o c_o u_3(L_C) \\ \rho_o c_o u_4(L_C) \end{bmatrix} = [\mathrm{E}(L_C)] \begin{bmatrix} kf_1 \\ kf_2 \\ kf_3 \\ kf_4 \\ kf_5 \\ kf_6 \end{bmatrix} \tag{29b}$$

Combining (29a) and (29b), the resultant relationship of the acoustic pressure and the particle velocity between x = 0 and x = Lc becomes

$$\begin{bmatrix} p_2(0) \\ p_3(0) \\ p_4(0) \\ \rho_o c_o u_2(0) \\ \rho_o c_o u_3(0) \\ \rho_o c_o u_4(0) \end{bmatrix} = \left[\mathrm{Y}\right] \begin{bmatrix} p_2(L_C) \\ p_3(L_C) \\ p_4(L_C) \\ \rho_o c_o u_2(L_C) \\ \rho_o c_o u_3(L_C) \\ \rho_o c_o u_4(L_C) \end{bmatrix} \tag{30a}$$

$$\text{where } \left[\mathrm{Y}\right] = \left[\mathrm{E}(0)\right]\left[\mathrm{E}(L_C)\right]^{-1} \tag{30b}$$

To obtain the transform matrix between the inlet (x = 0) and the outlet (x = Lc) of the inner tubes, four boundary conditions for the outer tube at x = 0 and x = Lc are placed in the calculation.

$$\frac{p_3(0)}{-u_3(0)} = -j\rho_o c_o \cot(kL_A) \tag{31a}$$

$$\frac{p_2(L_C)}{u_2(L_C)} = -j\rho_o c_o \cot(kL_B) \tag{31b}$$

$$\frac{p_3(L_C)}{u_3(L_C)} = -j\rho_o c_o \cot(kL_B) \tag{31c}$$

$$\frac{p_4(L_C)}{u_4(L_C)} = -j\rho_o c_o \cot(kL_B) \tag{31d}$$

By combining (31a)-(31d) with (30) and developing them, the transfer matrix yields

$$\begin{bmatrix} p_2(0) \\ \rho_o c_o u_2(0) \end{bmatrix} = \begin{bmatrix} TPRF2_{1,1} & TPRF2_{1,2} \\ TPRF2_{2,1} & TPRF2_{2,2} \end{bmatrix} \begin{bmatrix} p_4(L_C) \\ \rho_o c_o u_4(L_C) \end{bmatrix} \tag{32a}$$

or in a brief form

$$\begin{bmatrix} \overline{p}_2 \\ \rho_o c_o \overline{u}_2 \end{bmatrix} = \begin{bmatrix} TPRF2_{1,1} & TPRF2_{1,2} \\ TPRF2_{2,1} & TPRF2_{2,2} \end{bmatrix} \begin{bmatrix} \overline{p}_4 \\ \rho_o c_o \overline{u}_4 \end{bmatrix} \tag{32b}$$

where

$$\overline{p}_2 = p_2(0);\ \overline{u}_2 = u_2(0);\ \overline{p}_4 = p_4(L_C);\ \overline{u}_4 = -u_4(L_C);$$

$$TPRF2_{1,1} = \frac{H_{15}}{H_{17}};\ TPRF2_{1,2} = \frac{1}{\rho_o c_o} \cdot \left(\frac{H_{15}H_{18}}{H_{17}} - H_{16}\right);$$

$$TPRF2_{2,1} = \frac{\rho_o c_o}{H_{17}};\ TPRF2_{2,2} = \frac{H_{18}}{H_{19}};$$

$$K_{11} = \rho_o c_o[\mathrm{Y}_{14} - j\mathrm{Y}_{11}\cot(kL_B)];$$

$$K_{12} = \rho_o c_o[\mathrm{Y}_{15} - j\mathrm{Y}_{12}\cot(kL_B)];$$

$$K_{13} = \rho_o c_o[\mathrm{Y}_{16} - j\mathrm{Y}_{13}\cot(kL_B)];$$

$$K_{21} = \rho_o c_o[\mathrm{Y}_{24} - j\mathrm{Y}_{21}\cot(kL_B)];$$

$$K_{22} = \rho_o c_o[\mathrm{Y}_{25} - j\mathrm{Y}_{22}\cot(kL_B)];$$

$$K_{23} = \rho_o c_o[\mathrm{Y}_{26} - j\mathrm{Y}_{23}\cot(kL_B)];$$

$$K_{31} = \rho_o c_o[\mathrm{Y}_{34} - j\mathrm{Y}_{31}\cot(kL_B)];$$

$$K_{32} = \rho_o c_o[\mathrm{Y}_{35} - j\mathrm{Y}_{32}\cot(kL_B)];$$

$$K_{33} = \rho_o c_o[\mathrm{Y}_{36} - j\mathrm{Y}_{33}\cot(kL_B)];$$

$$K_{41} = \rho_o c_o[\mathrm{Y}_{44} - j\mathrm{Y}_{41}\cot(kL_B)];$$

$$K_{42} = \rho_o c_o[\mathrm{Y}_{45} - j\mathrm{Y}_{42}\cot(kL_B)];$$

$$K_{43} = \rho_o c_o[\mathrm{Y}_{46} - j\mathrm{Y}_{43}\cot(kL_B)];$$

$$K_{51} = \rho_o c_o[\mathrm{Y}_{54} - j\mathrm{Y}_{51}\cot(kL_B)];$$

$$K_{52} = \rho_o c_o[\mathrm{Y}_{55} - j\mathrm{Y}_{52}\cot(kL_B)];$$

$$K_{53} = \rho_o c_o[\mathrm{Y}_{56} - j\mathrm{Y}_{53}\cot(kL_B)];$$

$$K_{61} = \rho_o c_o[\mathrm{Y}_{64} - j\mathrm{Y}_{61}\cot(kL_B)];$$

$$K_{62} = \rho_o c_o[\mathrm{Y}_{65} - j\mathrm{Y}_{62}\cot(kL_B)];$$

$$K_{63} = \rho_o c_o[\mathrm{Y}_{66} - j\mathrm{Y}_{63}\cot(kL_B)];$$

$$H_1 = \frac{j\cot(kL_A)\cdot K_{52} - K_{22}}{K_{21} - jK_{51}\cot(kL_A)};\ H_2 = \frac{j\cot(kL_A)\cdot K_{53} - K_{23}}{K_{21} - jK_{51}\cot(kL_A)};$$

$$H_3 = K_{11}H_1 + K_{12};\ H_4 = K_{11}H_2 + K_{13};\ H_5 = K_{31}H_1 + K_{32};$$

$$H_6 = K_{31}H_2 + K_{33};\ H_7 = K_{41}H_1 + K_{42};\ H_8 = K_{41}H_2 + K_{43};$$

$$H_9 = K_{61}H_1 + K_{62};\ H_{10} = K_{61}H_2 + K_{63};\ H_{11} = \frac{\rho_o c_o H_{10}}{H_7 H_{10} - H_8 H_9};$$

$$H_{12}=\frac{-\rho_o c_o H_8}{H_7 H_{10}-H_8 H_9};\ H_{13}=\frac{\rho_o c_o H_9}{H_8 H_9-H_7 H_{10}};$$

$$H_{14}=\frac{-\rho_o c_o H_7}{H_8 H_9-H_7 H_{10}};\ H_{15}=H_3 H_{11}+H_4 H_{13};$$

$$H_{16}=H_3 H_{12}+H_4 H_{14};\ H_{17}=H_5 H_{11}+H_6 H_{13};$$

$$H_{18}=H_5 H_{12}+H_6 H_{14} \tag{32c}$$

3. Sound Transmission Loss

$$\begin{pmatrix}\bar{p}_1\\ \rho_o c_o \bar{u}_1\end{pmatrix}=e^{-jM_1 k(L_1+L_A)/(1-M_1^2)}\begin{bmatrix}TS1_{1,1} & TS1_{1,2}\\ TS1_{2,1} & TS1_{2,2}\end{bmatrix}\begin{pmatrix}\bar{p}_2\\ \rho_o c_o \bar{u}_2\end{pmatrix} \tag{33}$$

$$\begin{pmatrix}\bar{p}_2\\ \rho_o c_o \bar{u}_2\end{pmatrix}=\begin{bmatrix}TPRF2_{1,1} & TPRF2_{1,2}\\ TPRF2_{2,1} & TPRF2_{2,2}\end{bmatrix}\begin{pmatrix}\bar{p}_4\\ \rho_o c_o \bar{u}_4\end{pmatrix} \tag{34}$$

$$\begin{pmatrix}\bar{p}_4\\ \rho_o c_o \bar{u}_4\end{pmatrix}=e^{-jM_4 k(L_1+L_A)/(1-M_4^2)}\begin{bmatrix}TS3_{1,1} & TS3_{1,2}\\ TS3_{2,1} & TS3_{2,2}\end{bmatrix}\begin{pmatrix}\bar{p}_5\\ \rho_o c_o \bar{u}_5\end{pmatrix} \tag{35}$$

The total transfer matrix assembled by multiplication is

$$\begin{pmatrix}\bar{p}_1\\ \rho_o c_o \bar{u}_1\end{pmatrix}=e^{-jk\left[\frac{M_1(L_1+L_A)}{1-M_1^2}+\frac{M_4(L_1+L_A)}{1-M_4^2}\right]}\begin{bmatrix}TS1_{1,1} & TS1_{1,2}\\ TS1_{2,1} & TS1_{2,2}\end{bmatrix}\begin{bmatrix}TPFR2_{1,1} & TPRF2_{1,2}\\ TPRF2_{2,1} & TPRF2_{2,2}\end{bmatrix}\begin{bmatrix}TS3_{1,1} & TS3_{1,2}\\ TS3_{2,1} & TS3_{2,2}\end{bmatrix}\begin{pmatrix}\bar{p}_5\\ \rho_o c_o \bar{u}_5\end{pmatrix} \tag{36}$$

A simplified form in the matrix is expressed as

$$\begin{pmatrix}\bar{p}_1\\ \rho_o c_o \bar{u}_1\end{pmatrix}=\begin{bmatrix}T_{11}^* & T_{12}^*\\ T_{21}^* & T_{22}^*\end{bmatrix}\begin{pmatrix}\bar{p}_5\\ \rho_o c_o \bar{u}_5\end{pmatrix} \tag{37}$$

Under the assumption of a fixed thickness of the tubes ($t_1 = t_2 = 0.001$ m) and the symmetric design ($L_A = L_B = (L_Z - L_C)/2$), the sound transmission loss (*STL*) of a muffler is defined as [7]

$$STL\left(Q, f, Aff_1, Aff_2, Aff_3, Aff_4, dh_1, \eta_1, dh_2, \eta_2\right)=\log\left(\frac{\left|T_{11}^*+T_{12}^*+T_{21}^*+T_{22}^*\right|}{2}\right)+10\log\left(\frac{S_1}{S_5}\right) \tag{38a}$$

where

$Aff_1 = L_Z/L_o$; $Aff_2 = L_C/L_Z$; $Aff_3 = D_1/D_o$; $Aff_4 = D_2/D_o$;

$L_o = L_{Z4} + L_{Z5}$; $L_o = L_1 + L_Z$; $L_Z = L_A + L_B + L_C$;

$L_A = L_B = (L_Z\text{-}L_C)/2$ (38b)

4. Overall Sound Power Level

The silenced octave sound power level emitted from a silencer's outlet is

$$SWL_i = SWLO_i - STL_i \tag{39}$$

where (1) $SWLO_i$ is the original *SWL* at the inlet of a muffler (or pipe outlet), and *i* is the index of the octave band frequency.

(2) STL_i is the muffler's *STL* with respect to the relative octave band frequency.

(3) SWL_i is the silenced *SWL* at the outlet of a muffler with respect to the relative octave band frequency.

Finally, the overall SWL_T silenced by a muffler at the outlet is

$$SWL_T=10*\log\{\sum_{i=1}^{5}10^{SWL_i/10}\}$$
$$=10*\log\left\{\begin{array}{l}10^{[SWLO(f=125)-STL(f=125)]}+10^{[SWLO(f=250)-STL(f=250)]/10}\\+10^{[SWLO(f=500)-STL(f=500)]/10}+10^{[SWLO(f=1000)-STL(f=1000)]/10}+10^{[SWLO(f=2000)-STL(f=2000)]/10}\end{array}\right\} \tag{40}$$

5. Objective Function

By using the formulas of (38) and (40), the objective function used in the *GA* optimization was established.

1) STL Maximization for a One- Tone (f) Noise

$$OBJ_1 = STL\left(Q, f, Aff_1, Aff_2, Aff_3, Aff_4, dh_1, \eta_1, dh_2, \eta_2\right) \tag{41}$$

2) SWL Minimization for a Broadband Noise

To minimize the overall SWL_T, the objective function is

$$OBJ_2 = SWL_T\left(Q, Aff_1, Aff_2, Aff_3, Aff_4, dh_1, \eta_1, dh_2, \eta_2\right) \tag{42}$$

The related ranges of parameters are

$f = 300$ (Hz), Q = 0.01 (m^3/s); $D_o = 0.5$ (m), $L_o = 0.5$ (m);
Aff_1: [0.2, 0.8]; Aff_2: [0.2, 0.8]; Aff_3: [0.1, 0.3]; Aff_4: [0.1, 0.3];
η_1: [0.03, 0.1]; dh_1: [0.00175, 0.007]; η_2: [0.03, 0.1];
dh_2: [0.00175, 0.007] (43)

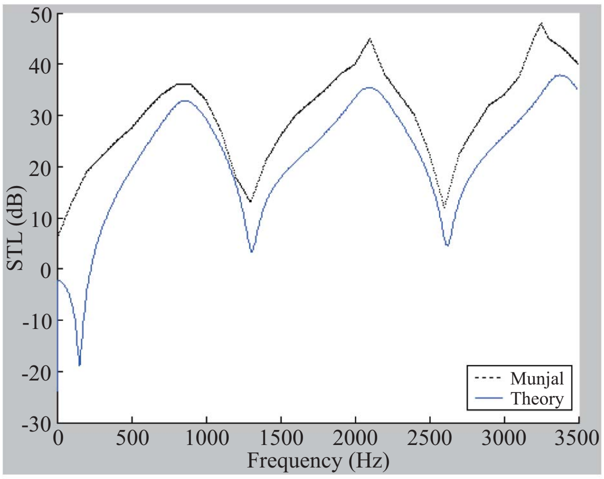

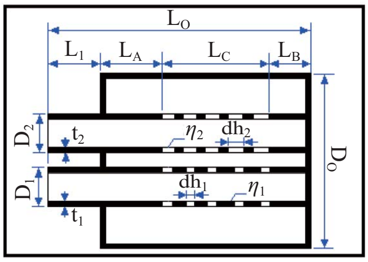

Fig. 7. Performance of a one-chamber reverse-flow perforated muffler [D_1 = 0.0493 (m), D_1 = 0.0493 (m), Do = 0.1481 (m), L_A = L_B = 0.0064, L_c = 0.1286 (m), t_1 = t_2 = 0.0081 (m), dh_1 = dh_2 = 0.0035 (m), η_1 = η_2 = 0.039, M_1 = 0.1] [Analytical data is from Munjal *et al.* [8]].

Table 1. Unsilenced *SWL* of an air compressor inside a duct outlet.

Frequency - Hz	125	250	500	1000	2000
SWLO - dB	120	125	118	105	100

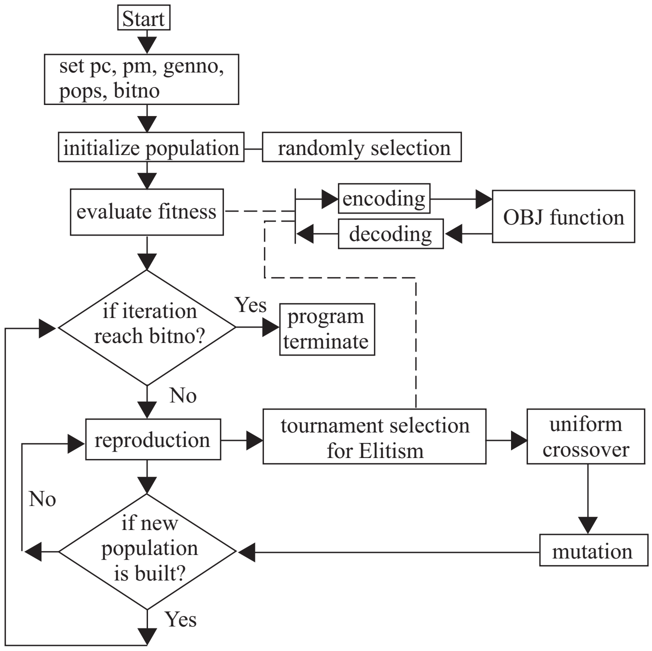

Fig. 8. Flow chart of the GA.

III. MODEL CHECK

Before performing the *GA* optimal simulation on mufflers, an accuracy check of the mathematical model on a one-chamber muffler with reverse-flow perforated tubes is performed by Munjal *et al.* [8]. As indicated in Fig. 7, the accuracy comparisons between theoretical data and analytical data are in agreement. Therefore, the model of one-chamber mufflers with reverse-flow and perforated tubes in conjunction with the numerical searching method is acceptable and adopted in the following optimization process.

IV. CASE STUDIES

In this paper, the noise reduction of a space-constrained air compressor is exemplified and shown in Fig. 1. The sound power level (*SWL*) inside the air compressor's outlet is shown in Table 1 where the overall *SWL* reaches 126.8 dB. To depress the huge venting noise emitted from the compressor's outlet, a one-chamber muffler hybridized with reverse-flow tubes is considered. To obtain the best acoustical performance within a fixed space volume, numerical assessments linked to a *GA* optimizer are applied. Before the minimization of a broadband noise is executed, a reliability check of the *GA* method by maximization of the *STL* at a targeted one tone (200 Hz) has been carried out. As shown in Figs. 1 and 2, the available space for a muffler is 0.5 m in width, 0.5 m in height, and 0.5 m in length. The flow rate (Q) and thickness of a perforated tube (t) are preset as 0.01 (m^3/s) and 0.001 (m), respectively; the corresponding *OBJ* functions, space constraints, and the ranges of design parameters are summarized in (41)~(43).

V. GENETIC ALGORITHM

The concept of Genetic Algorithms, first formalized by Holland [4] and then extended to functional optimization by D. Jong [5], involves the use of optimization search strategies patterned after the Darwinian notion of natural selection.

As the block diagram indicates in Fig. 8, the techniques of tournament selection, gene mutation, and the gene's uniform crossover are adopted in the *GA* process.

For the optimization of the objective function (*OBJ*), the design parameters of $(X_1, X_2,\ldots,X_k)$ were determined. When the *bitno* (the bit length of the chromosome) was chosen, the interval of the design parameter (X_k) with $[Lb, Ub]_k$ was then mapped to the band of the binary value. The mapping system between the variable interval of $[Lb, Ub]_k$ and the k^{th} binary chromosome of

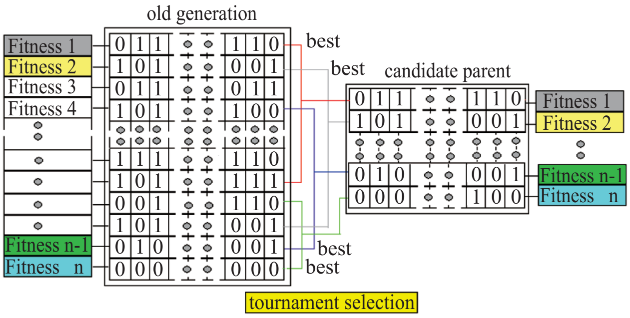

Fig. 9. Scheme of elitism by tournament selection.

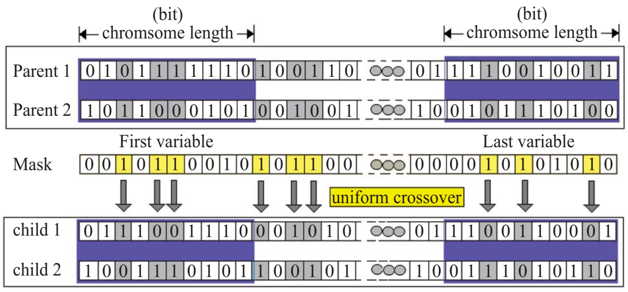

Fig. 10. Scheme of uniform crossover.

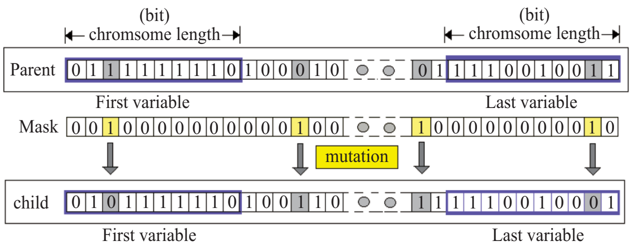

Fig. 11. Scheme of mutation.

$$[\underbrace{0\ \ 0\ \ 0\ \ 0\ \bullet\ \bullet\ \bullet\ 0\ \ 0\ \ 0}_{bit}\sim\underbrace{1\ \ 1\ \ 1\ \ 1\ \bullet\ \bullet\ \bullet\ 1\ \ 1\ \ 1}_{bit}]$$

was then built. The encoding from x to *B2D* (binary to decimal) can be performed as

$$B2D_k = \text{integer}\left\{\frac{x_k - Lb_k}{Ub_k - Lb_k}(2^{bit} - 1)\right\} \tag{44}$$

The initial population was built up by randomization. The parameter set was encoded to form a string which represented the chromosome. By evaluating the objective function (*OBJ*), the whole set of chromosomes [$B2D_1$, $B2D_2$, …., $B2D_k$] that changed from binary form to decimal form was then assigned a fitness by decoding the transformation system.

$$fitness = OBJ(X_1, X_2, \ldots, X_k) \tag{45a}$$

where

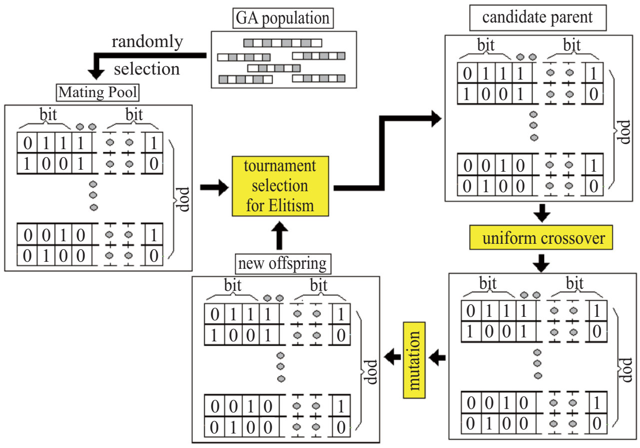

Fig. 12. Operations in the GA method.

$$X_k = B2D_k*(Ub_k\text{-}Lb_k)/(2^{bit}\text{-}1) + Lb_k \tag{45b}$$

As indicated in Fig. 9, to process the elitism of a gene, the tournament selection, a random comparison of the relative fitness of pairs of chromosomes, was applied. During the *GA* optimization, one pair of offspring from the selected parent was generated by uniform crossover with a probability of *pc*. The scheme of uniform crossover is shown in Fig. 10. Genetically, mutation occurred with a probability of *pm* where the new and unexpected point was brought into the *GA* optimizer's search domain. The scheme of mutation is shown in Fig. 11.

The process was terminated when a number of generations exceeded a pre-selected value of *genno*. The operations in the *GA* method are pictured in Fig. 12.

VI. RESULTS AND DISCUSSION

1. Result

To achieve good optimization, five kinds of *GA* parameters, including population size (*pops*), chromosome length (*bitno*), maximum generation (*genno*), crossover ratio (*pc*), and mutation ratio (*pm*) are varied step by step during optimization. The optimization system is encoded by Fortran and run on an IBM PC - Pentium IV. The results of two kinds of optimizations — one of the pure tone noises used for *GA*'s accuracy check and the other of broadband noise occurring in an air compressor room — are described below.

1) Pure Tone Noise Optimization

Twelve sets of *GA* parameters are tested by varying the values of the *GA* parameters. The simulated results with respect to the pure tone of 200 Hz is summarized and shown in Table 2. As indicated in Table 2, the optimal design data can be obtained from the last set of *GA* parameters at (*pops*, *bit*, *genno*, *pc*, *pm*) = (120, 15, 80, 0.9, 0.05). Using the optimal design in a theoretical calculation, the optimal *STL* curves with

Table 2. Optimal *STL* for a one-chamber muffler with reverse-flow ducts (at a targeted tone of 200 Hz).

Item	GA parameters					Results				
	Pops	*bitno*	*genno*	*pc*	*pm*					
1	60	10	20	0.3	0.05	*Aff*1	*Aff*2	*Aff*3	*Aff*4	*STL* (dB)
						*Aff*1	*Aff*2	*Aff*3	*Aff*4	35.8
						0.6757	0.7818	0.2263	0.1600	
						η_1	dh_1(m)	η_2	dh_2(m)	
2	60	10	20	0.6	0.05	*Aff*1	*Aff*2	*Aff*3	*Aff*4	*STL* (dB)
						0.7232	0.7859	0.1979	0.1772	37.8
						η_1	dh_1(m)	η_2	dh_2(m)	
						0.03609	0.00547	0.0917	0.00513	
3	60	10	20	**0.9**	**0.05**	*Aff*1	*Aff*2	*Aff*3	*Aff*4	*STL* (dB)
						0.6833	0.6205	0.1108	0.2486	40.3
						η_1	dh_1(m)	η_2	dh_2(m)	
						0.07393	0.00419	0.0854	0.00613	
4	60	10	20	0.9	0.03	*Aff*1	*Aff*2	*Aff*3	*Aff*4	*STL* (dB)
						0.7818	0.7085	0.2187	0.2554	31.0
						η_1	dh_1(m)	η_2	dh_2(m)	
						0.08009	0.00236	0.0415	0.00633	
5	60	10	20	0.9	0.07	*Aff*1	*Aff*2	*Aff*3	*Aff*4	*STL* (dB)
						0.7038	0.7877	0.1393	0.1882	35.2
						η_1	dh_1(m)	η_2	dh_2(m)	
						0.08385	0.00191	0.0913	0.00677	
6	90	10	20	0.9	0.05	*Aff*1	*Aff*2	*Aff*3	*Aff*4	*STL* (dB)
						0.7208	0.7707	0.1233	0.2801	36.5
						η_1	dh_1(m)	η_2	dh_2(m)	
						0.09446	0.00254	0.0755	0.00259	
7	120	10	20	0.9	0.05	*Aff*1	*Aff*2	*Aff*3	*Aff*4	*STL* (dB)
						0.7994	0.7836	0.1049	0.1663	32.7
						η_1	dh_1(m)	η_2	dh_2(m)	
						0.08597	0.00300	0.0970	0.00432	
8	**120**	**15**	20	0.9	0.05	*Aff*1	*Aff*2	*Aff*3	*Aff*4	*STL* (dB)
						0.7994	0.7930	0.1538	0.1166	57.2
						η_1	dh_1(m)	η_2	dh_2(m)	
						0.09124	0.00291	0.0729	0.00530	
9	120	20	20	0.9	0.05	*Aff*1	*Aff*2	*Aff*3	*Aff*4	*STL* (dB)
						0.7900	0.7202	0.1297	0.1409	47.5
						η_1	dh_1(m)	η_2	dh_2(m)	
						0.09836	0.00232	0.0761	0.00280	
10	120	25	20	0.9	0.05	*Aff*1	*Aff*2	*Aff*3	*Aff*4	*STL* (dB)
						0.7050	0.7707	0.1037	0.2648	37.5
						η_1	dh_1(m)	η_2	dh_2(m)	
						0.09898	0.00261	0.0768	0.00636	
11	120	10	40	0.9	0.05	*Aff*1	*Aff*2	*Aff*3	*Aff*4	*STL* (dB)
						0.7971	0.7994	0.1022	0.1000	60.6
						η_1	dh_1(m)	η_2	dh_2(m)	
						0.09610	0.00358	0.0895	0.00513	
12	**120**	**10**	**80**	**0.9**	**0.05**	*Aff*1	*Aff*2	*Aff*3	*Aff*4	*STL* (dB)
						0.7988	**0.7947**	**0.1913**	**0.2429**	62.1
						η_1	dh_1(m)	η_2	dh_2(m)	
						0.09685	**0.00195**	**0.0344**	**0.00517**	

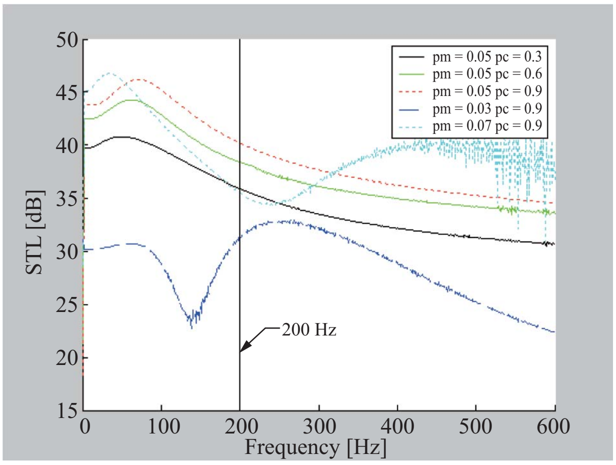

Fig. 13. *STL* with respect to frequency at various *pc* and *pm* [target tone of 200 Hz] [at *pops* = 60, *bitno* = 10, *genno* = 20].

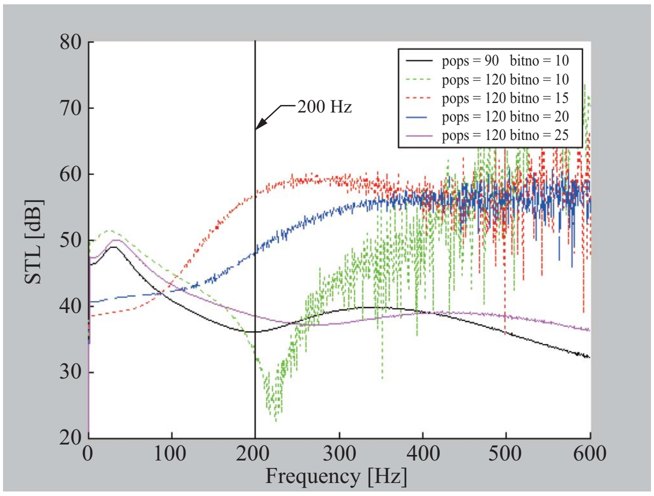

Fig. 14. *STL* with respect to frequency at various *pops* and *bitno* [target tone of 200 Hz] [at *pc* = 0.9, *pm* = 0.05, *genno* = 20].

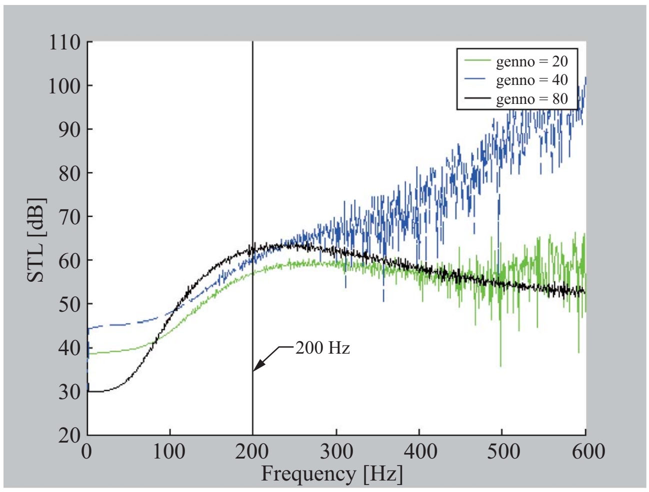

Fig. 15. *STL* with respect to frequency at various *genno* [target tone of 200 Hz] [at *pc* = 0.9, *pm* = 0.05, *pops* = 120, *bitn0* = 15].

Table 3. Optimal *SWL* for a one-chamber muffler with reverse-flow ducts (for a broadband noise).

GA parameters					Results				
Pops	*bitno*	*genno*	*pc*	*pm*					
120	10	80	0.9	0.05	*Aff*1	*Aff*2	*Aff*3	*Aff*4	SWL_T (dB)
					0.7994	0.7883	0.2007	0.1178	82.9
					η_1	dh_1(m)	η_2	dh_2(m)	
					0.09063	0.004218	0.06421	0.003048	

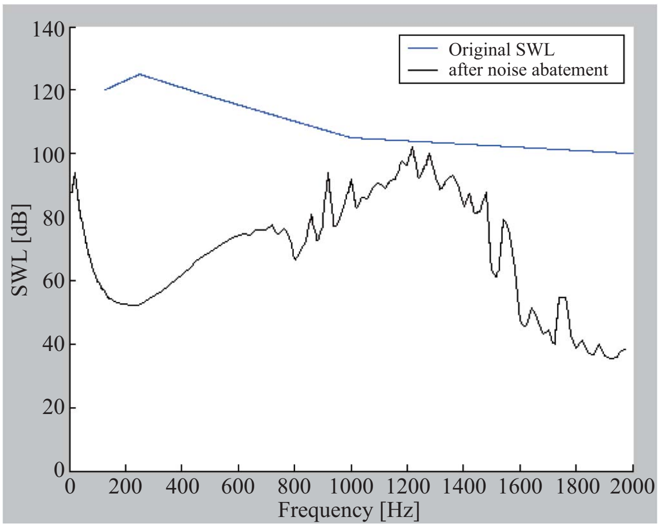

Fig. 16. *SWL* with respect to frequency [broadband noise] [at *pc* = 0.9, *pm* = 0.05, *pops* = 120, *bitn0* = 15, *genno* = 80].

respect to various *GA* parameters are plotted and depicted in Figs. 13-15. As revealed in Figs. 13-15, the *STL*s are precisely maximized at the desired frequencies.

2) Broadband Noise Optimization

By using the above *GA* parameters, the muffler's optimal design data for one-chamber mufflers hybridized with reverse-flow perforated ducts used to minimize the sound power level at the muffler's outlet is summarized in Table 3. As illustrated in Table 3, the resultant sound power levels with respect to three kinds of mufflers have been dramatically reduced from 126.8 dB(A) to 82.9 dB(A). Using this optimal design in a theoretical calculation, the resultant *SWL* before and after adding the muffler at the outlet is shown in Fig. 16. As shown in Fig. 16, the muffler has the best acoustical performance. Based on plane wave theory, the proposed available theoretical cutoff frequencies of fc_1 $\left(f_{c1} = \frac{1.84 c_o}{\pi D}(1-M^2)^{1/2} \right)$ is 2002 Hz.

2. Discussion

To achieve a sufficient optimization, the selection of the appropriate *GA* parameters set is essential. As indicated in Table 2, the best *GA* set at the targeted pure tone noise of 200 Hz has been shown. Using the appropriate *GA* set at the targeted pure tone (200 Hz), the related optimal *STL* curves are plotted in Figs. 13-15. The Figs. 13-15 reveal the predicted maximal value of the *STL* is precisely located at the desired frequency. Therefore, using the *GA* optimization in finding a better design solution is reliable; moreover, in dealing with the broadband noise, the *GA*'s solution shown in Table 3 and Fig. 16 can also provide the appropriate and sufficient sound reduction under space-constraint conditions. As can be observed in Table 3, the overall sound transmission loss of the one-chamber muffler with reverse-flow perforated ducts reaches 43.9 dB.

VII. CONCLUSION

It has been shown that one-chamber mufflers hybridized with reversed-flow and perforated ducts can be easily and efficiently optimized within a limited space by using a generalized decoupling technique, a plane wave theory, a four-pole transfer matrix, as well as a *GA* optimizer. Five kinds of *GA* parameters (*pops, genno, bitno, pc, pm*) play essential roles in the solution's accuracy during *GA* optimization. As indicated in Figs. 13-15, the tuning ability established by adjusting design parameters of mufflers is reliable. In addition, the appropriate acoustical performance curve of one-chamber mufflers with reverse-flow and perforated ducts in depressing overall broadband noise has been assessed. As indicated in Table 3 and Fig. 16, the overall sound transmission loss of mufflers reaches 43.9 dB. Consequently, the approach used for the optimal design of the *STL* proposed in this study is indeed easy and quite effective.

ACKNOWLEDGMENTS

The author acknowledges the financial support of the National Science Council (NSC 95-2218-E-235-002, ROC)

REFERENCES

1. Chang, Y. C., Yeh, L. J., and Chiu, M. C., "Numerical studies on constrained venting system with side inlet/outlet mufflers by GA optimization," *Acta Acustica united with Acustica*, Vol. 90, No. 1-1, pp. 1-11 (2004).
2. Chang, Y. C., Yeh, L. J., and Chiu, M. C., "Shape optimization on double-chamber mufflers using genetic algorithm," *Proceedings ImechE Part C: Journal of Mechanical Engineering Science*, Vol. 10, pp. 31-42 (2005).
3. Davis, D. D., Stokes, J. M., and Moorse, L., "Theoretical and experimental investigation of mufflers with components on engine muffler design," *NACA Report*, pp. 1192 (1954).
4. Holland, J., *Adaptation in Natural and Artificial System*, Ann Arbor, University of Michigan Press (1975).
5. Jong, D., *An Analysis of the Behavior of a Class of Genetic Adaptive Systems*, Doctoral thesis, Dept. Computer and Communication Sciences, Ann Arbor, University of Michigan (1975).
6. Magrab, E. B., *Environmental Noise Control*, John Wiley & Sons, New York (1975).

7. Munjal, M. L., *Acoustics of Ducts and Mufflers with Application to Exhaust and Ventilation System Design*, John Wiley & Sons, New York (1987).
8. Munjal, M. L., Rao, K. N., and Sahasrabudhe, A. D., "Aeroacoustic analysis of perforated muffler components," *Journal of Sound and Vibration*, Vol. 114, No. 2, pp. 173-188 (1987).
9. Peat. K. S., "A numerical decoupling analysis of perforated pipe silencer elements," *Journal of Sound and Vibration*, Vol. 123, No. 2, pp. 199-212 (1988).
10. Rao, K. N. and Munjal, M. L., "Experimental evaluation of impedance of perforates with grazing flow," *Journal of Sound and Vibration*, Vol. 123, pp. 283-295 (1986).
11. Sullivan, J. W., "A method of modeling perforated tube muffler components I: theory," *Journal of the Acoustical Society of America*, Vol. 66, pp. 772-778 (1979).
12. Sullivan, J. W., "A method of modeling perforated tube muffler components II: theory," *Journal of the Acoustical Society of America*, Vol. 66, pp. 779-788 (1979).
13. Sullivan, J. W. and Crocker, M. J., "Analysis of concentric tube resonators having unpartitioned cavities," *Journal of the Acoustical Society of America*, Vol. 64, pp. 207-215 (1978).
14. Thawani, P. T. and Jayaraman, K., "Modeling and applications of straight-through resonators," *Journal of the Acoustical Society of America*, Vol. 73, No. 4, pp. 1387-1389 (1983).
15. Yeh, L. J., Chang, Y. C., and Chiu, M. C., "Numerical studies on constrained venting system with reactive mufflers by GA optimization," *International Journal for Numerical Methods in Engineering*, Vol. 65, pp. 1165-1185 (2006).
16. Yeh, L. J., Chang, Y. C., Chiu, M. C., and Lai, G. J., "Computer-aided optimal design of a single-chamber muffler with side inlet/outlet under space constraints," *Journal of Marine Science and Technology*, Vol. 11, No. 4, pp. 1-8 (2003).